American Journal of Pathology, Vol. 168, No. 1, January 2006

DOI: 10.2353/ajpath.2006.050443

Tumorigenesis and Neoplastic Progression

Differential Sensitivity of Mouse Epithelial Tissues to the Polyomavirus Middle T Oncogene

Grace Cecena,* Fang Wen,* Robert D. Cardiff,*† and Robert G. Oshima*

From the Oncodevelopmental Biology Program, Cancer Research Center, The Burnham Institute, La Jolla; and the Center for Comparative Medicine,† Department of Pathology, University of California at Davis, Davis, California*

To determine how different epithelial cell types respond to the same oncogenic stimulation, we have used a modified human keratin 18 gene to conditionally express the polyomavirus middle T antigen (PyMT) oncogene in simple epithelial tissues of transgenic mice. Activation of PyMT expression by transgenic Cre recombinase in mammary epithelial cells resulted in carcinomas in all bitransgenic females. PyMT expression induced by K18-driven Cre in internal epithelial organs resulted in pancreatic acinar metaplasia and ductal dysplasia with remarkable desmoplastic stromal responses in all 25 bitransgenic mice. Hepatoma formation with altered lipid metabolism and gastric adenocarcinoma occurred in 96 and 54% of these mice, respectively. Elevated PyMT RNA expression also correlated with intraepithelial neoplasia in the prostate. Activated Erk2 was found in mammary tumors, pancreatic tissues, and affected livers. Hes1 RNA, a target of Notch signaling that has been implicated downstream of Ras pathway activation, was elevated in pancreatic and liver lesions. The variety of responses of different epithelia to PyMT demonstrates the importance of the differentiated state in interpreting oncogenic signals. ***(Am J Pathol 2006, 168:310–320; DOI: 10.2353/ajpath.2006.050443)***

Oncogenes generally stimulate normal cells to proliferate. However, the cellular response to a particular oncogene and the mechanism by which growth is stimulated may vary with the differentiated type and state of the tissue. Ras and phosphatidylinositol-3′ kinase (PI3′K) signal transduction pathways have been implicated in breast cancer to provide mitotic stimulation, to provide protection from apoptosis, and to stimulate angiogenesis. The polyomavirus middle T antigen (PyMT) is a compact and efficient oncogene that stimulates multiple signal transduction pathways by interacting with Shc, Src, PI3′K, and protein phosphatase 2A. The simultaneous activation of the Shc/Ras/Erk and PI3′K/Akt pathways by PyMT results in mammary tumors with RNA expression profiles that are the same as those caused by activated Neu/ErbB2.[1] The histopathological and molecular characteristics of the progression of PyMT-induced tumors have been shown to closely resemble human breast cancer.[2–4] Thus, the expression of PyMT in mammary epithelial tissue of the adult provides a well-characterized and potent oncogenic stimulation of signaling pathways known to be important in human cancers. Previous attempts to test PyMT in epithelial tissues of transgenic mice have been limited by lethality and unpredictable integration site effects.[5–8] Here, we have used the K18 gene as an expression vector because of its predictable behavior yielding epithelial-specific expression in transgenic mice that is largely integration site independent.[9,10] We have tested the potency of PyMT in activating Ras and PI3′K pathways and in eliciting cancer in pancreas, liver, stomach, prostate, and mammary gland, and we show that these organs respond differently to the expression of the same oncogene.

Materials and Methods

Transgene Construction

The KFS2MT vector was constructed by standard cloning and polymerase chain reaction (PCR) methods starting with the K18 gene[11] and the K18iresAP[9] and pUC.A.1.5[12] plasmids. Sequence of the vector is available on request. The KFS2MT vector was digested with *Sal*I and *Nae*I to release a 13,121-bp transgene fragment containing 282 bp of plasmid vector sequence.

Supported by National Cancer Institute grants P01 CA102583 and RO1CA42302 to R.G.O., Cancer Center Support grant CA30199 at the Burnham Institute, U42 RR14905 from the National Institutes of Health/National Center for Research Resources, and R01 CA89140 to R.D.C. at the University of California, Davis.

Accepted for publication September 20, 2005.

Address reprint requests to Robert G. Oshima, 10901 North Torrey Pines Road, La Jolla, CA 92037. E-mail: rgoshima@burnham.org.

Transgenic Mice

The purified transgene fragment was injected into FVB/N strain mouse zygotes as described previously[13,14] by Dr. Ling Wang of the Burnham Institute Mouse Genetics Laboratory Shared Resource. Transgenic mice were identified by PCR of tail lysate DNA. MMTV-Cre7 mice[15] were provided by Dr. William Muller (McGill University, Montreal, Canada). PB-Cre4 mice[16] were provided by Dr. Roy-Burman through the National Cancer Institute Mouse Models of Human Cancer Consortium. K18CreER^{T2}-20 (K18CreER) mice and treatment with 5-hydroxytamoxifen (OHT) were described previously.[9] Cre transgenic mice were identified by PCR. Recombination of the loxP sequences of KFS2MT was verified by PCR of *Bgl*II-digested purified organ DNA. All mice were of the FVB/N genetic background except PB-Cre4, which was on a C57Bl/6 background. Only F_1 KFS2MT6; PB-Cre4 bitransgenic mice were analyzed in this report. Sequences of all PCR primers used for construction of the vector and for genotype determination are available on request.

Trophoblast Stem Cell Culture

Trophoblast stem cells were isolated by culturing individual mouse blastocysts as described previously.[17] The AdCreGFP virus coding for Cre recombinase and green fluorescent protein (GFP) was a gift from Dr. Serguei V. Kozlov. Virus was generated in low-passage 293 cells according to the supplier's instructions (Microbix Biosystems, Toronto, Canada).

DNA and mRNA Analysis

Quantitative, reverse transcriptase-dependent PCR (Q-PCR) was performed on a Stratagene MX3000 machine using the SYBR Green detection method as described previously.[18] Southern blots were performed as described previously.[19] Pancreatic tissues used for RNA isolation were stored in RNA Later (Ambion Inc., Austin, TX). RNA was isolated with the use of Tri-reagent (Molecular Research Center, Cincinnati, OH).

Tissue Analysis

Tissues were fixed with 4% paraformaldehyde or 10% formalin, dehydrated, embedded in paraffin, sectioned, and stained with hematoxylin and eosin by standard methods. *In situ* hybridization was performed on paraffin-embedded tissues as described previously.[20] Antibody staining for PyMT and estrogen receptor (ER) was performed as described previously.[21,22]

Protein Analysis

Frozen tumors and tissues were homogenized in 2× cell lysis buffer (catalog no. 9803; Cell Signaling Technology, Beverly, MA) containing a 1/200 dilution of protease inhibitor cocktail (catalog no. 8340; Sigma-Aldrich, St. Louis, MO). Protein contents of the cleared supernatants were determined using the Bio-Rad protein assay (catalog no. 500-0006; Bio-Rad, Hercules, CA); and for kinase assays, 10 μg of protein was separated by sodium dodecyl sulfate-polyacrylamide gel electrophoresis. Protein was transferred to 0.45-μm polyvinylidene difluoride membrane (Immobilon; Millipore, Billerica, MA). Filters were blocked, washed, and probed as recommended by the antibody supplier. Antibody reaction was detected using horseradish peroxidase (HRP)-linked rabbit secondary antibody (catalog no. P0217; Dako, Carpinteria, CA) diluted 1:2000 in Tris-HCl buffered saline, 0.1% Tween-20 (TBS-T) and 5% (w/v) nonfat dry milk and detected by ECL plus chemiluminescent detection according to the manufacturer's instructions (Amersham Biosciences, Piscataway, NJ). Antibodies from Cell Signaling Technology were used at 1:1000 for phospho-p44/42 MAP kinase antibody (catalog no. 9101), Erk1/2 (p44/42 MAP kinase antibody; catalog no. 9102), phospho-Akt (Thr308; catalog no. 9275), and Akt (catalog no. 9272). For PyMT protein analysis, 20 μg of protein per sample was used. Filters were blocked with 5% (w/v) nonfat dry milk and incubated with a 1:2000 dilution of rat anti PyMT antibody[21,22] in 3% bovine serum albumin in TBS-T for 2 hours. After washing with TBS-T, primary antibody was revealed with HRP-labeled donkey anti-rat IgG (1:20,000) (catalog no. 712-035-135; Jackson ImmunoResearch, West Grove, PA) and ECL reagent. Tubulin was detected on stripped filters with mouse anti-α-tubulin (catalog no. T6199; Sigma) used at 1:10,000 dilution, followed by HRP-labeled anti-native mouse IgG (TruBlot; catalog no. 18-8877; eBioscience, San Diego, CA) at 1:1000 and ECL reagent.

Results

Cre-Dependent PyMT Expression from the K18 Gene

To obtain conditional epithelial-specific expression, we modified the 10-kb K18 gene that is expressed in adult simple epithelial organs.[9,10] Three repeated elements of the SV40 early region polyadenylation signals with flanking LoxP recombination sites were inserted into the first exon, preventing expression of the transgene in the absence of Cre recombinase (Figure 1A). PyMT was placed downstream of an internal ribosome entry sequence (IRES) within the K18 gene.[9] Three mouse lines carrying the KFS2MT transgene, designated KFS2MT1, KFS2MT4, and KFS2MT6, contained one, two, or three copies of the transgene, respectively (data not shown). Trophoblast stem cells derived from two lines expressed elevated PyMT RNA after infection with Cre-expressing adenovirus. This confirmed Cre-dependent activation of the integrated transgene (data not shown).

KFS2MT6-Induced Mammary Tumors

To test the latency and specific induction of PyMT, the KFS2MT6 line was combined with each of three different transgenic mouse lines that express Cre recombinase.

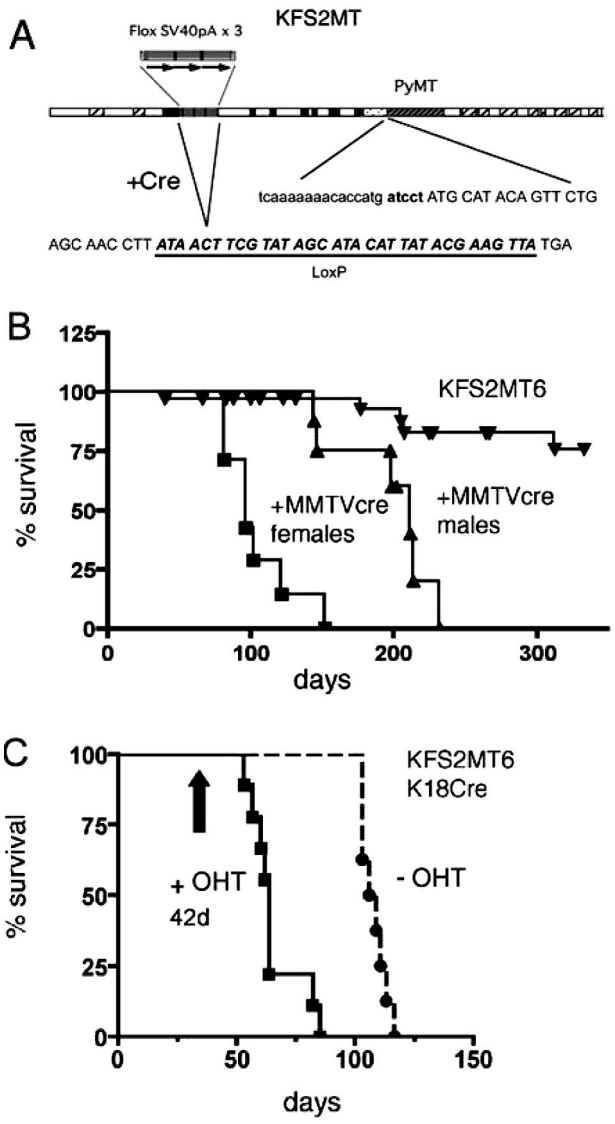

Figure 1. KFS2MT6 survival. **A:** Map of the KFS2MT transgene. Coding exons of the human K18 gene are shown in **black**. **Hatched rectangles** indicate alu sequences. **Dotted region** indicates the position of the IRES. The sequence of the junction between the IRES and the PyMT coding sequence is shown. Three copies of the SV40 termination sequences are indicated with **arrows**. The action of Cre recombinase results in the deletion of the termination signals and leaves a single loxP sequence with two translational termination codons. **B** and **C:** Kaplan-Meier plots of animals sacrificed because of noticeable alterations in appearance or behavior or found dead. Log-rank test indicated significant differences between all pairs of data. **Vertical arrow** indicates OHT administrations starting at 42 ± 2 days for 5 consecutive days. **B:** Bigenic KFS2MT6; MMTV-Cre7 bigenic females and males are compared to monogenic stock. **C:** Bigenic KFS2MT6; K18CreER animals were treated with OHT. −OHT, untreated animals.

The MMTV-Cre7 transgene is expressed primarily in the luminal epithelial cells of the mammary gland.[15] The PB-Cre4 transgenic line expresses Cre specifically in prostate epithelium.[16] The K18CreER expresses Cre fused to a mutant estrogen receptor ligand binding domain in a variety of internal epithelia and is activated by exposure to OHT.[9]

All KFS2MT6; MMTV-Cre7 bigenic females developed mammary tumors with a median age of 102 days (Figure 1B; Table 1). Mammary lesions of KFS2MT6; MMTV-Cre7 bigenic females ranged from small hyperplastic nodules (Figure 2A) to multiple cystic and papillary tumors, occasionally with pulmonary metastasis (Figure 2B). Generally, the tumors resembled previously described tumors arising because of the expression of PyMT variants.[23] Immunohistochemistry confirmed PyMT protein in the tumor cells (Figure 2C). ER was detected in a minority of KFS2MT6; MMTV-Cre7 mammary tumor cells in a mosaic pattern (Figure 2D). Most of the cells of solid tumors were negative for ER. Primarily, nuclear localization was detected, and generally sparse stromal staining was found. This distribution of ER is generally similar to advanced MMTV-PyMT tumors.[3,21]

Two female bigenic animals also developed focal differentiated hepatomas (Table 1). However, the hepatomas and a pancreatic lesion in one animal were not life threatening, unlike the large mammary tumors. Male KFS2MT6; MMTV-Cre7 mice survived longer until 199 days of age but commonly developed hepatic and pancreatic dysplastic lesions, prostate intraepithelial neoplasia (PIN), and bulbouretheral gland adenomas (Figure 1B; Table 1). These abnormalities were seen only in bigenic animals but not in KFS2MT6 mice, indicating modest ectopic expression of the MMTV-Cre7 transgene in the affected internal organs.

PyMT-Induced Pancreatic Dysplasia and Hepatic Neoplasms

To test the oncogenic potential of PyMT in a large number of internal epithelial tissues, the KFS2MT6 transgene was combined with the previously characterized K18CreER transgene. KFS2MT6; K18CreER bitransgenic mice of both sexes treated with OHT developed severe liver and pancreatic lesions requiring sacrifice at an average age of 66 days (Figure 3, C and E) or about 14 days after completion of drug treatment. Bigenic animals treated with vehicle alone or no treatment developed similar disease but not until an average age of 109 days, reflecting a low level of Cre activity in the absence of OHT activation. The weight of pancreas from drug-treated animals increased extremely rapidly (Figure 3A), reaching an average of sevenfold larger than controls (Figure 3C). The livers of the same animals were 70% larger than monogenic KFS2MT6 animals treated with OHT. The longer life span of bigenic animals treated only with vehicle or not treated resulted in more severe liver enlargement (Figure 3, B and D) and increased pancreas size (Figure 3, A and C). Combining KFS2MT6 with either prostate-specific PB-Cre4 or mammary gland-biased MMTV-Cre7 in females generally resulted in liver and pancreas of normal weight (Figure 3, A–D).

PyMT-Induced Liver Neoplasms

Livers of KFS2MT6; K18CreER bigenic animals had small to large expansile foci of hepatocytes of enlarged size with highly vacuolated cytoplasm (Figure 2, E and H). Staining with Oil Red O revealed that these vacuoles accumulated large amounts of lipid (Figure 2F). This was

Table 1. KFS2MT6 Affected Organs

PyMT Gene	KFS2MT6	KFS2MT6	KFS2MT6	KFS2MT6	KFS2MT6	KFS2MT6
Cre Gene		MMTV-Cre7	MMTV-Cre7	PBCre	K18CreER	K18CreER
Background	FVB/N	FVB/N	FVB/N	FVB/B6 F1	FVB/N	FVB/N
Sex	13m/23f	f	m	m	3m/6f	4m/12f
Total	36	7	6	8	9	16
Treatment					OHT	Oil/none
Stomach	0	0	0	0	5/8	9/16
Mammary gland	1	7/7	1/6	0/7	0/4	6/12
Liver	0/5	2/7	3/6	1/7	8/9	16/16
Pancreas	0/5	1/7	3/6	0/7	9/9	16/16
Prostate	0	na	4/6	4/7	2/3	1/4
Bulbourethral gland	0	na	4/6	2/7	0	0
Latency (days)	>360	82 to 152	147 to 232	174 to 300	53 to 85	60 to 117

The number of animals with pathological changes in the indicated organs and the total number of examined animals are listed (affected/total). Standard hematoxylin- and eosin-stained sections or carmine-stained whole mounts (mammary gland) were examined. f, female; m, male; na, not applicable.

also reflected by increased serum low-density lipoprotein in KFS6MT; K18CreER bigenic animals (18.2 ± 9.8 mg/dl, $n = 6$) compared with monogenic controls (7 ± 2 mg/dl, $n = 3$). *In situ* hybridization confirmed the correspondence between hepatocyte dysplasia and PyMT RNA expression (Figure 2G).

Pancreatic Alterations in Differentiated State

Pancreatic lesions from KFS2MT6; K18CreER bigenic animals appeared as foci of dysplastic ducts and increased, reactive stroma (Figure 4A) that embedded increasingly abnormal ductal structures (Figure 4B). The ductal structures in these foci had a high mitotic index with numerous abnormal mitoses. Pancreatic acinar tumors also developed, sometimes adjacent to the ductal foci (Figure 4C). Some ductal structures appeared specialized, resembling intestinal-like epithelium, perhaps reflecting an altered progenitor-differentiated state (Figure 4D). In many cases the entire pancreas appeared to have been replaced by dense fibrous connective tissue that contained a combination of distorted proliferating ducts and glands with increasing nuclear pleomorphism and abnormal mitotic figures. These more aggressive patterns were interpreted as neoplastic. Although most microscopic fields lacked islets, serum chemistry from several affected animals did not detect elevated serum glucose levels, suggesting that the animals were not insulin deficient at sacrifice. PyMT RNA and protein were associated with the ductal structures of the pancreatic lesions (Figure 4, E and H). Estrogen receptor protein was found in the pancreatic ductal structures in a mosaic pattern (Figure 4I). Dysplastic cells had a combination of nuclear and cytoplasmic staining. Focal lesions in younger or moderately affected animals (Figure 4A), the association of vacuoles with dysplastic acini (Figure 4, G and H), and increased PyMT associated with ducts (Figure 4H) suggest that acinar metaplasia may be an early event as previously described when activated Ras is expressed in acinar cells.[24] The response of pancreatic epithelial cells to PyMT may reflect a general dedifferentiation to less specialized epithelial cells.

PyMT-Induced Gastric Adenocarcinoma

KFS2MT6; K18CreER mice developed malignant, invasive adenocarcinomas of the stomach (Table 1; Figure 4, M and N). The number of animals with gastric cancers was likely limited by the necessity for sacrifice due to pancreatic and liver disease, because foci of dysplastic epithelial crypts were present in multiple animals without overt tumors. The association of ER expression with the epithelial components was somewhat surprising (Figure 4O). In this case, the ER stain was located in the cytoplasm and not the nucleus. No obvious histological abnormalities of colon were apparent in samples from 12 mice.

PIN

Bigenic KFS2MT6; K18CreER males developed prostate neoplasia ranging from PINI to PINIII with possible microinvasion (Figure 4, J and K). In the prostate, like in the pancreas, the epithelial lesions were accompanied by remarkable connective tissue proliferation (Figure 4J, black arrow). *In situ* hybridization confirmed PyMT RNA expression in affected prostate epithelia (Figure 4L). Activation of the KFS2MT6 in prostate epithelium was achieved more specifically by using the PB-Cre4 transgene (Table 1). Four of seven male bigenic KFS2MT6; PB-Cre4 mice developed PIN over a period of up to 300 days. However, prostate lesions were generally not invasive, and comparable disease development appeared a few weeks after OHT treatment of KFS2MT6; K18CreER male mice. The induction of epithelial organ lesions including prostate was not a characteristic exclusive to the KFS2MT6 line, because bigenic animals of the KFS2MT1 and KFS2MT4 transgenic lines generated similar abnormalities when combined with the PB-Cre4 or K18CreER transgenes (data not shown).

Molecular Analysis of PyMT-Induced Lesions

Southern blot and genomic PCR analysis of the KFS2MT6 transgene confirmed the expected MMTV-Cre7-medi-

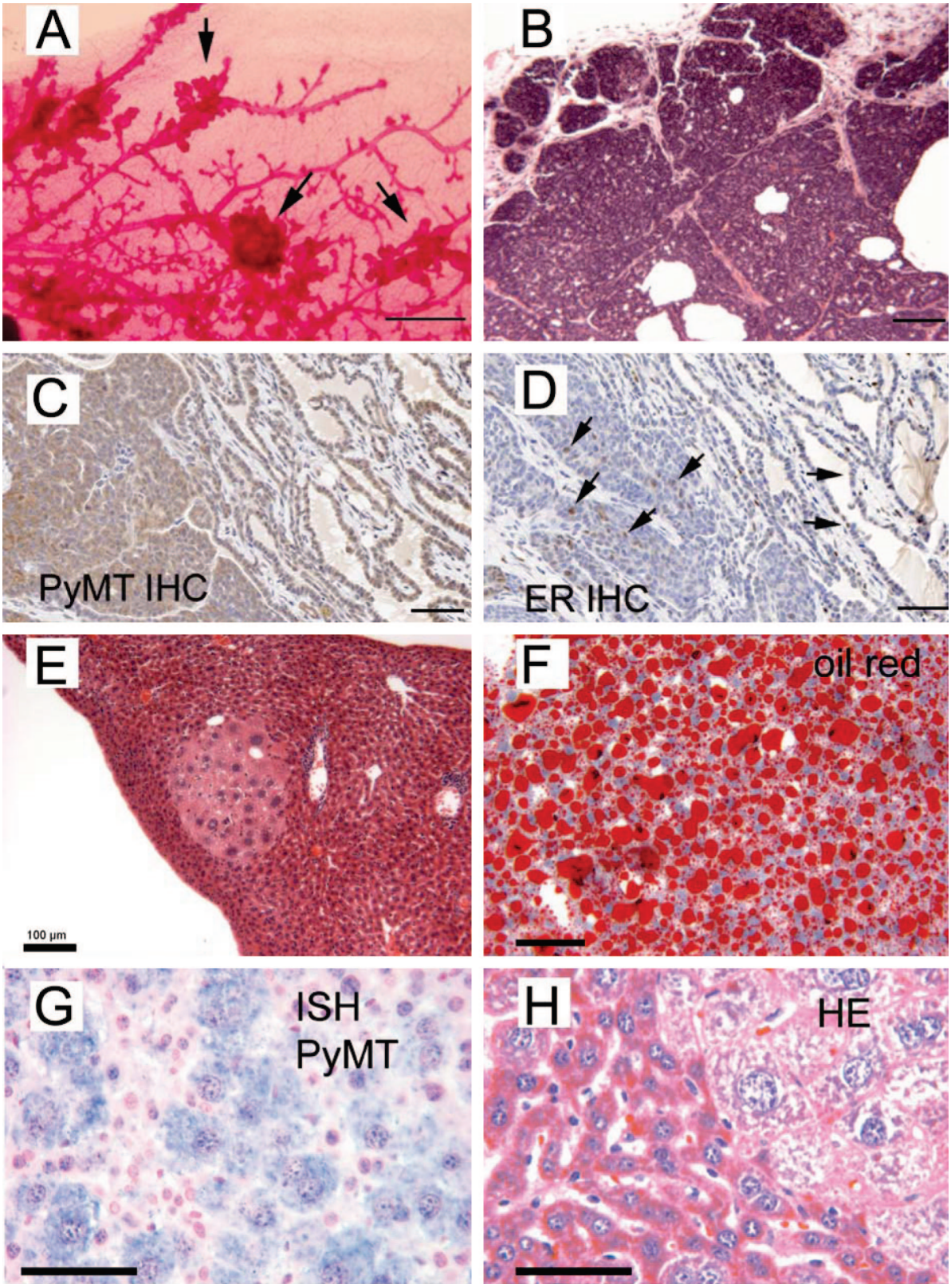

Figure 2. Histopathology of mammary lesions in KFS2MT6; MMTV-Cre7 females and livers from KFS2MT6; K18CreER bigenic mice. **A:** Whole mount, carmine-stained mammary gland from a 102-day-old mouse. **Arrows** point to epithelial hyperplastic nodules. Bar = 1 mm. **B:** Hematoxylin and eosin (HE)-stained section of a mammary tumor showing glandular growth of high cellular density from a 62-day-old bigenic female. **C:** Immunohistochemical detection of PyMT in a mammary tumor. Brown color indicates antibody reaction product. Note stronger stain in solid tumor areas at lower left quadrant and less in epithelial portion in upper right quadrant. **D:** Immunohistochemical detection of ER in a mammary tumor. **Arrows** indicate individual cells with positive nuclear stain. **E:** HE section of an affected liver with focal area of dysplastic hepatocytes. **F:** Oil red-O stain of frozen section of a bigenic liver. **G:** ISH of PyMT RNA in a bigenic liver. Swollen, dysplastic hepatocytes are positive for PyMT RNA. **H:** HE section of liver showing the interface between a focal lesion and normal liver. Bars in **B** through **E** = 100 μm. Bars in **F** through **H** = 50 μm.

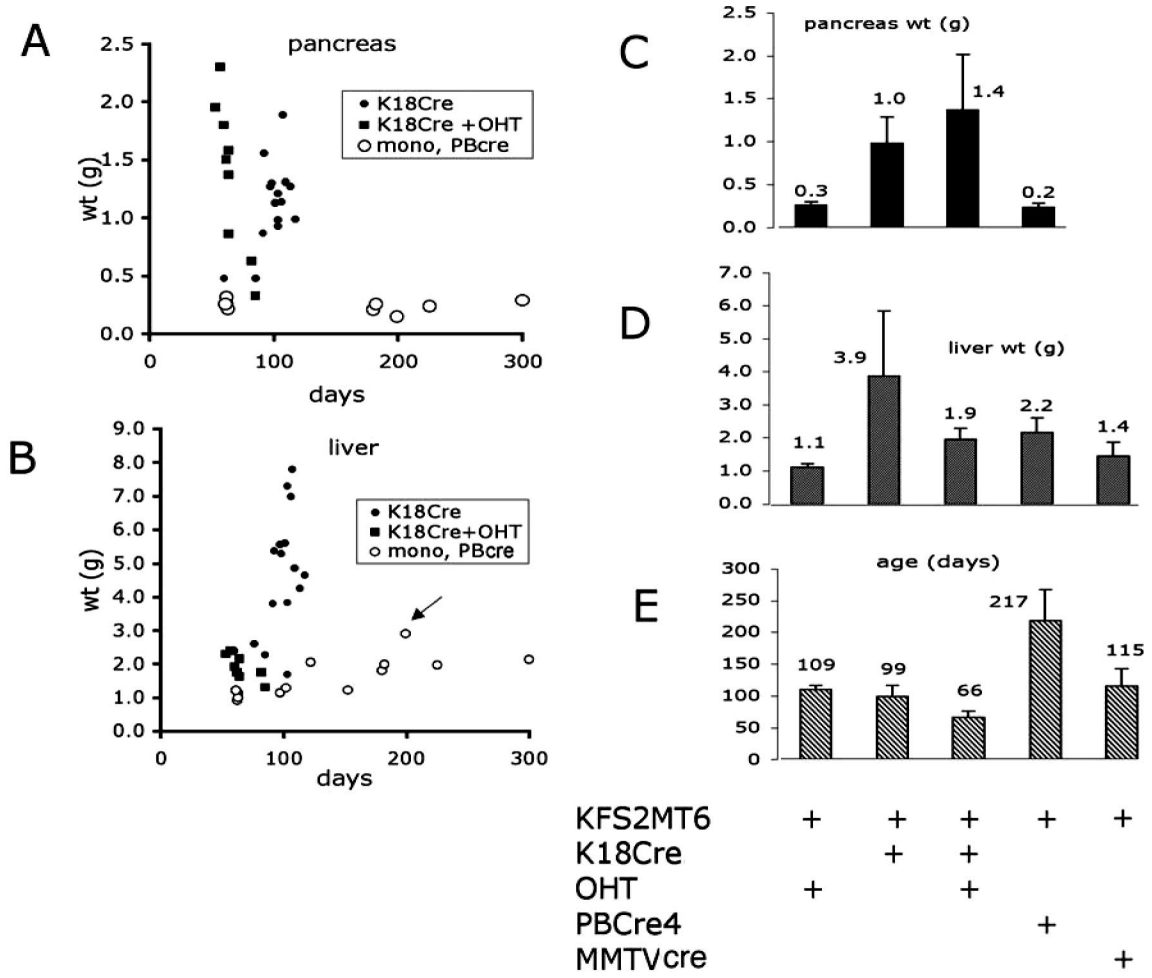

Figure 3. Pancreas and liver weights at time of sacrifice. **A:** Weights of pancreas of individual animals sacrificed at the indicated age. Each animal contained the KFS2MT6 transgene alone (mono) or in combination with K18CreER (K18Cre) or PB-Cre4 (PBCre) transgenes. Animal treated with OHT for 5 consecutive days are indicated. **B:** Individual weights of livers as indicated for **A**. In addition, MMTV-Cre7 (MMTVCre) transgene was combined with KFS2MT6. **Arrow** indicates the only liver of this MMTV-Cre7 series that had hepatic pathology. **C:** Average pancreas weight. Error bars indicate standard deviations. Genotype of the groups is indicated below **E**. **D:** Average liver weights as indicated for **C**. **E:** Average age at sacrifice. Error bars indicate standard deviations. The presence of four transgenes and OHT treatment are indicated at the bottom.

ated, 0.8-kb deletion in mammary tumors (Figure 5, A and B, lanes 9–10, and C, lanes 2–5). The intensity of the signal of the 1.5-kb recombined allele was similar to the native 2.3-kb fragment (Figure 5B, lane 6). This suggests that the Cre-mediated recombination did not delete intervening copies of the KFS2MT6 transgene array of three gene copies. The smaller recombined genomic fragment is represented less abundantly in male bigenic KFS2MT6; MMTV-Cre7 liver and pancreas, indicating that only a portion of sampled cells had undergone recombination (Figure 5B, lanes 3, 4, 7, and 8). Genomic PCR amplification of the recombination junction was consistent with most copies of the stop signals being removed in the mammary tumors (Figure 5C, lanes 2–4). Similarly, only weak bands corresponding to the recombined allele were detected in affected liver and pancreas from bigenic male animals. These results are consistent with a minority of cells with activated KFSMT6 transgenes causing the focal pathological lesions found in liver and pancreas and the majority of cells within the mammary tumors being recombined. These results confirmed the expected deletion of the stop signals associated with PyMT expression.

Cre-Dependent PyMT RNA Expression

KFS2MT6 adult tissues had undetectable to low levels of PyMT RNA (Figure 6A). Mammary tumors contained elevated PyMT RNA expression. However, expression levels were 40 times lower than tumors generated by the well-characterized MMTV-driven PyMT model (Figure 6A).[25] PyMT RNA levels were particularly elevated in bulbourethral gland tumors and pancreatic tumors. PyMT RNA expression correlated with lesions or frank tumors in both male and female KFS2MT6; MMTV-Cre7 mice. PyMT RNA was elevated in the colon despite the absence of obvious pathological lesions. In liver, PyMT RNA was 25-fold higher than control KFS2MT6 liver, comparable with bigenic pancreas, and higher than mammary tumors (Figure 6A).

The ductal metaplasia found in KFS2MT6; K18CreER pancreas is consistent with a dedifferentiated state. Be-

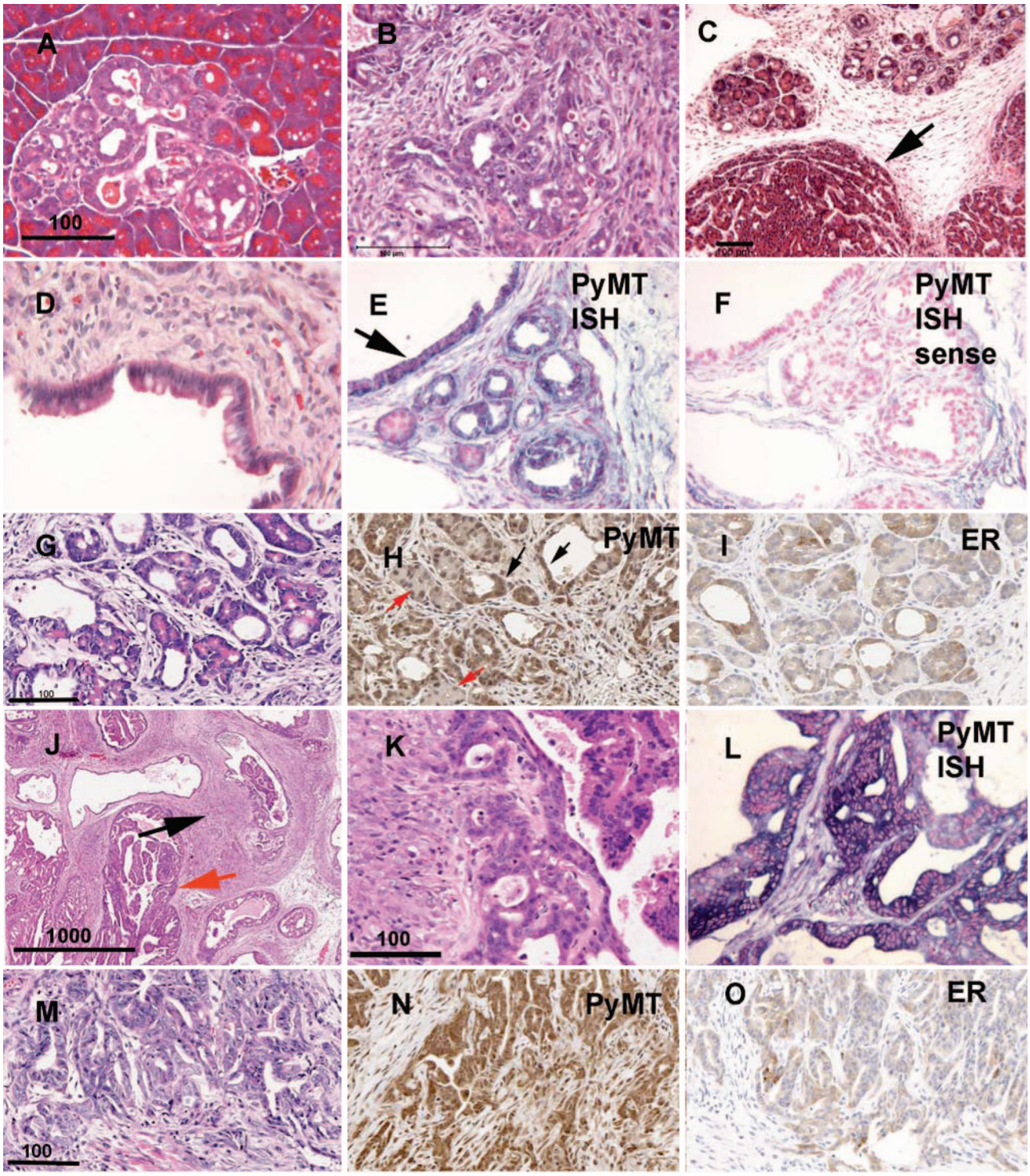

Figure 4. Histopathology of pancreatic, prostate, and stomach lesions of KFS2MT6; K18CreER mice. **A:** A focal area of pancreatic dysplasia in bigenic animal not treated with tamoxifen. Bar = 100 μm. **B:** Typical field of desmoplastic, dysmorphogenic pancreatic tumor. **C:** Acinar type tumor. **Arrow** points to border of acinar tumor and stromal area with embedded residual acini. **D:** Intestine-like differentiation within pancreatic tumor duct. **E:** ISH detection of PyMT RNA in dysplastic pancreatic epithelia. Blue color indicates PyMT RNA. Nuclear red counter stain. **Arrow** indicates differentiated epithelium as in **D**. **F:** ISH control with PyMT sense probe. Note stromal background reaction. **G:** HE-stained section of pancreas showing association of residual eosinophilic, acinar like cells with lumen vacuoles. Bar = 100 μm for **G**, **H**, and **I**. **H:** Immunohistochemical detection of PyMT associated with duct-like structures (**black arrows**) and weaker staining associated with residual acinar like cells (**red arrows**). **I:** Immunohistochemical detection of estrogen receptor with increased reaction associated with ductal structures. **J:** Low-magnification field of HE-stained prostate section showing remarkable stromal reaction (**black arrow**), intraepithelial neoplasia, and papillary proliferation (**red arrow**). Bar = 1 mm. **K:** Higher magnification of PIN region. Bar = 100 μm for **K** and **L**. **L:** PyMT ISH showing expression (blue color) of the oncogene in the epithelial cells of the prostate counter stained with nuclear red. **M:** HE-stained section of stomach adenocarcinomas found in a 64-day-old KFS2MT6; K18CreER bigenic male that was treated with tamoxifen. Bar = 100 μm. **N:** Immunohistochemical detection of PyMT in stomach adenocarcinomas. **O:** Estrogen receptor expression associated with stomach adenocarcinomas. Note that ER reaction appears to be primarily cytoplasmic.

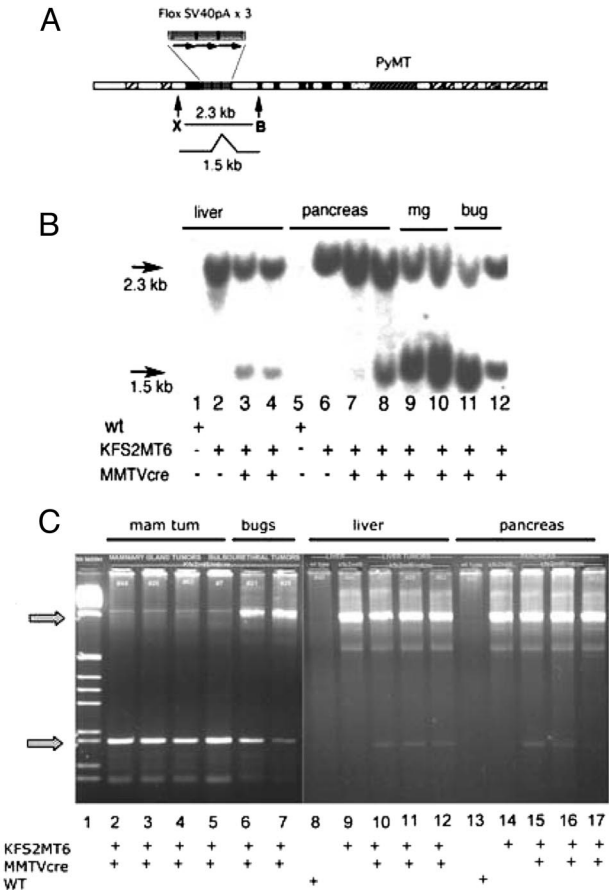

Figure 5. Cre-dependent transgene recombination. **A:** Map of KFS2MT transgene showing a 2.3-kb *Xho*I (X) to *Bgl*II (B) fragment that is shortened to 1.5 kb by Cre-mediated deletion of triplet-repeated SV40Pa elements. **B:** Southern blot analysis of KFS2MT6 alone and in combination with MMTV-Cre7 transgene as indicated at bottom of panel. DNAs isolated from liver, pancreas, mammary tumors (mg), and bulbourethral gland (bug) were digested with *Xho*I and *Bgl*II and detected by hybridization with a 250-bp probe (AF179904: 2576–2825) synthesized by PCR. The recombined (1.5 kb) form of the gene was detected in **lanes 3**, **4**, and **7** to **12**. Note the strength of the signal of the 1.5-kb form of the mammary tumors of **lanes 9** and **10** are similar to the monogenic control of **lane 6**. **C:** Genomic PCR confirmation of Cre-dependent recombination. Genomic DNA isolated from the indicated tumors or organs was subjected to PCR with primers flanking the floxed stop signals. This resulted in a larger fragment (**arrow**) of 1 kb (**top arrow**) for a nonrecombined transgene or a 0.2-kb fragment (**bottom arrow**) for a Cre-mediated recombination event. Note the abundance of the 0.2-kb PCR product in mammary tumors (mam tum) and bulbourethral gland tumors (bugs) and weak lower band in KFS2MT6; MMTV-Cre7 bigenic liver and pancreas.

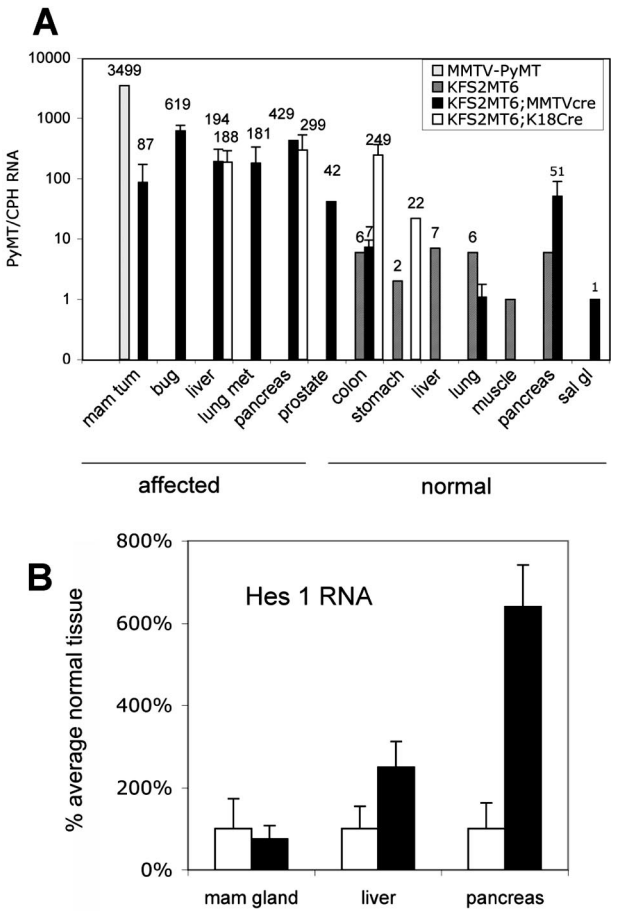

Figure 6. RNA expression in KFS2MT6 monogenic and bigenic tissues and tumors. **A:** PyMT RNA levels determined by Q-PCR are normalized to cyclophilin A RNA. MMTV-PyMT indicates average value of two independent mammary tumors. Bug, bulbourethral gland tumors; lung met, single value for a mammary-type tumor found in KFS2MT6; MMTV-Cre7 bigenic mouse lung; mam tum, mammary tumor; sal gl, salivary gland. Average values are shown. Error bars indicate standard deviations of values with three or more tumors. Labels below tissue names indicate appearance of organ at collection. **B:** Relative Hes1 and cyclophilin A RNA levels were determined by Q-PCR and are displayed relative to normal tissues. Each value represents the average of three to eight samples each from different mice. **Filled bars** indicate average values for bitransgenic tissues from KFS2MT6; MMTV-cre7 for mammary gland tumors and KFS2MT6; K18CreER animals for pancreatic tumors and livers.

cause Notch signaling has been implicated in pancreatic differentiation and in pancreatic cancer,[26] we measured RNA for Hes1, one target of Notch signaling (Figure 6B). Compared with levels found in normal pancreas from control or KFS2MT6 monogenic mice, Hes1 RNA was elevated approximately 6-fold in pancreatic tumors and 2.5-fold in hepatomas but not in mammary gland tumors. Thus, the activation of Notch signaling targets by comparable levels of PyMT is tissue dependent.

IRES-Dependent PyMT Protein Expression

PyMT protein expression was correlated with RNA levels in the tumors of bigenic KFS2MT6 mammary gland, liver, and pancreas (Figure 7A). As expected from the RNA levels, PyMT protein was much lower in KFS2MT6; MMTV-Cre7 tumors than MMTV-PyMT mammary tumors (Figure 7A, lane 2). Bigenic colon tissue had little or no detectable PyMT protein despite very elevated levels of RNA (Figure 6A). This suggests that the IRES of the KFS2MT6 mRNA may not be used efficiently in colon. The absence of PyMT protein in bigenic colon was consistent with the absence of pathological effect.

Erk Activation in KFS2MT6; MMTV-Cre7 Mammary Tumors

PyMT expression is expected to stimulate Src, Ras, and PI3′K signal transduction pathways. The activation states of Erk1/2 were compared in tumors derived from KFS2MT6; MMTV-Cre7 and MMTV-PyMT by Western

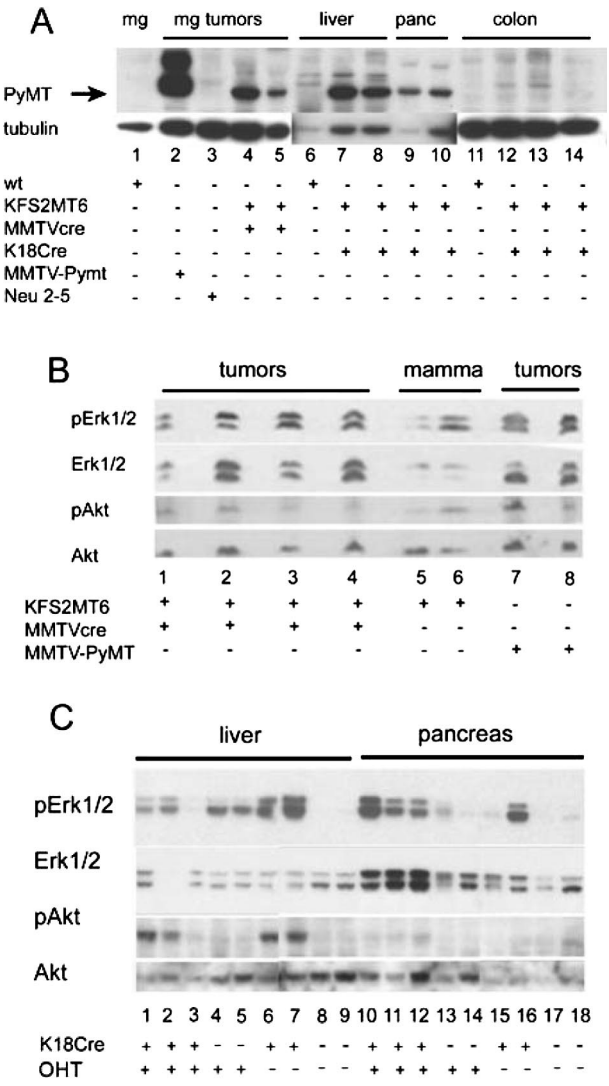

Figure 7. A: PyMT protein expression in tumors. PyMT and β-tubulin were detected by Western blot analysis. The filter was first reacted with PyMT antibody then stripped and reprobed for tubulin. Twenty micrograms of protein was loaded in each lane except for **lane 2**, which received 2 μg. The tubulin exposure of **lanes 6** to **10** was 5 minutes, whereas the remainder of the image represents a 0.5-minute exposure of the same filter. The genotypes of the animals from which the tissues were derived are shown at the bottom. Neu 2–5, represents line MMTV-Neu^{ndl2-5}.[28] mg, mammary gland; panc, pancreas. **B:** Frozen mammary tumors and normal whole mammary fat pad (mamma) were subjected to Western blot analysis. Genotype of the tissues is indicated at the bottom. Each lane contains tissue or tumor protein from a different animal. pErk1/2, phospho-Erk1 and phospho-Erk2. pAkt, phosphorylated form of Akt. **C:** Liver and pancreatic tissues from KFS2MT6 mice with additional genes or treatment indicated below lane numbers. K18Cre indicates presence of K18CreER transgene. OHT indicates 5-day treatment with 5-hydroxy-tamoxifen. Note increased pAkt in bigenic KFS2MT6; K18Cre liver (**lanes 1**, **2**, **6**, and **7**) and increase pErk1/2 in bigenic KFS2MT6; K18CreER in pancreas (**lanes 10** to **12**).

blotting. The relative levels of phosphorylated Erk1/2 were comparable in KFS2MT6; MMTV-Cre7 and MMTV-PyMT tumors despite the 40-fold differences in PyMT RNA (Figure 7B, lanes 1–4, 7, and 8). Phosphorylated levels of Erk1/2 were surprisingly high in mammary fat pads of monogenic KFS2MT6 females (Figure 7B, lanes 5 and 6). However, the abundance of nonepithelial tissue in virgin whole mammary fat pad makes a direct comparison with tumor tissue potentially misleading. These results suggest that stimulation of Erk1/2 may be maximal in mammary tumors and that further stimulation is not achieved by higher expression of PyMT in MMTV-PyMT tumors. As a surrogate for PI3′K activity, we measured the degree of phosphorylation of Akt, a downstream target of PI3′K. P-Akt levels of KFS2MT6; MMTV-Cre7 tumors were similar to MMTV-PyMT tumors.

PyMT Activation of Akt in Liver and Erk in Pancreas

The phosphorylated forms of Erk1 and Erk2 were increased in the livers of KFS2MT6; K18CreER bigenic animals (Figure 7C, lanes 1, 2, 6, and 7) relative to normal liver (Figure 7C, lanes 8 and 9). However, pErk1/2 were also elevated in livers of tamoxifen-treated monogenic KFS2MT6 mice approximately 2 weeks after termination of drug treatment (Figure 7C, lanes 4 and 5). Either the drug or the metabolism of the oil vehicle may stimulate Erk1/2 phosphorylation independent of PyMT expression. Erk2 was preferentially phosphorylated, relative to Erk1 in liver and pancreas. In contrast to pErk2 elevation in KFS2MT6 livers by tamoxifen treatment, pAkt levels were elevated in four of five livers of bigenic animals (Figure 7C, lanes 1–3, 6, and 7). The levels of pAkt (Figure 7C, lanes 10–12, 15, and 16) did not exceed normal pancreas (Figure 7C, lanes 17 and 18), even though pancreata of four of five bigenic animals contained elevated levels of pErk2. Elevated pErk1/2 levels in KFS2MT6; MMTV-Cre7 mammary tumors and KFS2MT6; K18CreER livers and pancreata are consistent with stimulation by PyMT expression. However, pAkt levels in pancreas did not reveal a sustained activation by PyMT expression.

Discussion

The extensive analysis of PyMT provides a firm molecular foundation for understanding a potent oncogenic stimulus independent of p53.[27] The indistinguishable RNA expression profiles of mammary tumors caused by PyMT and by activated Neu provides strong support for the view that PyMT activates the same pathways as Neu and ErbB3 signaling in the mammary gland.[1,28,29] The response of different epithelial tissues to PyMT expression differed in regard to aggressiveness, metastasis, and differentiated state. The differential induction of Hes1, a Notch signaling pathway target, reinforces cell type-specific differences in response to PyMT. However, all tissue that expressed elevated PyMT protein exhibited at least premalignant changes. The histological similarity of KFS2MT6; MMTV-Cre7 mammary tumors to previously described PyMT mammary tumors occurs despite significantly less PyMT RNA expression.[30,31] This may be due to maximal activation of signaling pathways by overexpressed PyMT in both systems, as reflected by the similar levels of pErk1/2 in both types of mammary tumors. However, KFS2MT6; MMTV-Cre7 tumors were more heterogeneous than MMTV-PyMT tumors with greater squamous metaplasia. This pattern correlated with less

intense PyMT staining and was previously associated with mammary tumors caused by the Wnt pathway.[30] The greater variation in tumor organization and PyMT expression may be, in part, due to the transcriptional stimulation of the K18 gene by Ras pathway activation.[32] This potential positive-feedback regulation may also support the explosive pancreatic growth associated with OHT activation of KFS2MT6; K18CreER.

In pancreas, epithelial expression of PyMT resulted in ductal and glandular dysplasia with extensive stromal expansion and occasional acinar tumors. The abundance of ductal structures appears similar to preinvasive lesions caused by elastase-driven K-ras expression,[24] Pdx1-Cre-induced K-ras expression,[33] and pancreatic expression of transforming growth factor-α in the presence of inactive p53.[34] However, KFS2MT6; K18CreER pancreatic lesions did not progress to invasive cancers within the maximal 4-month life of the bigenic animals. The pancreatic lesions contrast with the expression of PyMT in pancreas by avian retrovirus delivery that resulted in occult lesions unless they were combined with Ink4a/Arf deficiency.[35] These differences between the KFS2MT6 and viral-delivered PyMT may be due to the difference in cellular targets and higher sustained expression from the recombined KFS2MT6 vector. K18 is expressed in acinar and ductal cells, whereas the replication-competent avian leukosis viral long terminal repeat with splice acceptor virus was targeted largely to acinar cells by the elastase-driven TVA receptor.

The response of liver to PyMT was distinct from that of both pancreas and mammary gland. Hepatomas formed because of increased mitotic activity and increased cell size. Portal tract deficiency was also consistent with a neoplastic state. Expression of PyMT in liver, as in mammary gland, did not stimulate the stromal response characteristic of pancreas and prostate. Thus, the response of liver to PyMT was neoplastic with secondary metabolic or differentiated function alterations. The commonality between the different responses of mammary gland, liver, pancreas, and prostate may be an alteration in the state of differentiation. The increase in pancreatic Hes1 RNA in KFS2MT6; K18CreER animals is consistent with this idea. Notch signaling controls Hes1 expression and Hes1 inhibits the differentiation of pancreatic progenitor cells.[36,37] In pancreas, Notch signaling and targets like Hes1 appear to mediate pancreatic metaplasia caused by transforming growth factor-α stimulation of the Ras signal transduction pathway.[26] Thus, it is likely that Ras pathway activation by PyMT may also cause acinar metaplasia through Hes1 expression.

In prostate, expression of PyMT from either the KFS2MT6 or KFS2MT4 lines and activated by either K18CreER or PB-Cre4 resulted in intraepithelial neoplasia and remarkable desmoplastic response. However, the PIN lesions progressed relatively slowly. Previously, expression of PyMT in prostate was associated with lethal prostate cancer, and mammary and bronchioalveolar tumors when driven by the C3(1) gene promoter.[38] Expression levels of PyMT in this previous trial may have been at significantly higher levels than achieved from the K18 gene vector. However, PyMT RNAs in affected prostates of KFS2MT6; MMTV-Cre7, KFS2MT6; PB-Cre4, or KFS2MT4; PB-Cre4 males were only modestly lower than KFS2MT6; MMTV-Cre7 mammary tumors. Thus, the slow progression of prostate PIN may reflect an intrinsic, differentiation state-dependent sensitivity and response to PyMT.

Although PyMT binds PI3′K and has been shown to activate downstream Akt, we did not find evidence for elevated pAkt in pancreas. The tissue-specific modulation of pAkt may be mediated by particularly high protein phosphatase 2A activity, by high PTEN activity, or by more indirect mechanisms. Clearly, pancreas and liver have distinct, integrated responses to PyMT expression. PyMT has been investigated extensively because of its transforming activity. However, PyMT does not cause tumors in rodent hosts within the context of the normal virus lifecycle.[27] A variety of tumors arise only when high titer virus is inoculated in newborn animals of certain strains of mice. The normal function of PyMT to alter the differentiated state of lung Clara cells to optimize virus replication may also be reflected by the varied responses of different epithelial cell types tested here.

We have shown previously that transgenic expression of MMTV-driven Neu and vascular endothelial growth factor have overlapping but not identical patterns of expression within mammary epithelial cells.[20] In combination with MMTV-Cre7, KFS2MT6 may be of particular value for the evaluation of mammary tumor cell autonomous effects of any floxed gene. In addition, the rapid kinetics of pancreatic lesions in KFS2MT6; K18CreER mice after OHT treatment may make this model attractive for a number of applications.

Acknowledgments

We thank Robbin Newlin for technical help with histology, the personnel of the Burnham Institute Animal Facility for careful assistance with animal husbandry, and the histology staff at the U.C. Davis Center for Comparative Medicine, Mutant Mouse Pathology Laboratory.

References

1. Desai KV, Xiao N, Wang W, Gangi L, Greene J, Powell JI, Dickson R, Furth P, Hunter K, Kucherlapati R, Simon R, Liu ET, Green JE: Initiating oncogenic event determines gene-expression patterns of human breast cancer models. Proc Natl Acad Sci USA 2002, 99:6967–6972
2. Cardiff RD, Rosner A, Hogarth MA, Galvez JJ, Borowsky AD, Gregg JP: Validation: the new challenge for pathology. Toxicol Pathol 2004, 32(Suppl 1):31–39
3. Lin EY, Jones JG, Li P, Zhu L, Whitney KD, Muller WJ, Pollard JW: Progression to malignancy in the polyoma middle T oncoprotein mouse breast cancer model provides a reliable model for human diseases. Am J Pathol 2003, 163:2113–2126
4. Namba R, Maglione JE, Young LJ, Borowsky AD, Cardiff RD, MacLeod CL, Gregg JP: Molecular characterization of the transition to malignancy in a genetically engineered mouse-based model of ductal carcinoma in situ. Mol Cancer Res 2004, 2:453–463
5. Williams RL, Courtneidge SA, Wagner EF: Embryonic lethalities and endothelial tumors in chimeric mice expressing polyoma virus middle T oncogene. Cell 1988, 52:121–131
6. Sabapathy KT, Pepper MS, Kiefer F, Mohle-Steinlein U, Tacchini-Cottier F, Fetka I, Breier G, Risau W, Carmeliet P, Montesano R,

Wagner EF: Polyoma middle T-induced vascular tumor formation: the role of the plasminogen activator/plasmin system. J Cell Biol 1997, 134:953–963
7. Rassoulzadegan M, Courtneidge SA, Loubiere R, el Baze P, Cuzin F: A variety of tumours induced by the middle T antigen of polyoma virus in a transgenic mouse family. Oncogene 1990, 5:1507–1510
8. Aguzzi A, Wagner EF, Williams RL, Courtneidge SA: Sympathetic hyperplasia and neuroblastomas in transgenic mice expressing polyoma middle T antigen. New Biol 1990, 2:533–543
9. Wen F, Cecena G, Munoz-Ritchie V, Fuchs E, Chambon P, Oshima RG: Expression of conditional cre recombinase in epithelial tissues of transgenic mice. Genesis 2003, 35:100–106
10. Oshima RG, Baribault H, Caulin C: Oncogenic regulation and function of keratin 8 and 18. Cancer Metastasis Rev 1996, 15:445–471
11. Kulesh DA, Oshima RG: Cloning of the human keratin 18 gene and its expression in non-epithelial mouse cells. Mol Cell Biol 1988, 8:267–272
12. Maxwell IH, Harrison GS, Wood WM, Maxwell F: A DNA cassette containing a trimerized SV40 polyadenylation signal which efficiently blocks spurious plasmid-initiated transcription. BioTechniques 1989, 7:276–280
13. Abe M, Oshima RG: A single human keratin 18 gene is expressed in diverse epithelial cells of transgenic mice. J Cell Biol 1990, 111:1197–1206
14. Thorey IS, Meneses J, Neznanov N, Kulesh D, Pedersen R, Oshima RG: Embryonic expression of human keratin 18 and K18-beta-galactosidase fusion genes in transgenic mice. Dev Biol 1993, 160:519–534
15. Andrechek ER, Hardy WR, Siegel PM, Rudnicki MA, Cardiff RD, Muller WJ: Amplification of the neu/erbB-2 oncogene in a mouse model of mammary tumorigenesis. Proc Natl Acad Sci USA 2000, 97:3444–3449
16. Wu X, Wu J, Huang J, Powell WC, Zhang J, Matusik RJ, Sangiorgi FO, Maxson RE, Sucov HM, Roy-Burman P: Generation of a prostate epithelial cell-specific Cre transgenic mouse model for tissue-specific gene ablation. Mech Dev 2001, 101:61–69
17. Tanaka S, Kunath T, Hadjantonakis AK, Nagy A, Rossant J: Promotion of trophoblast stem cell proliferation by FGF4. Science 1998, 282:2072–2075
18. Galang CK, Muller WJ, Foos G, Oshima RG, Hauser CA: Changes in the expression of many Ets family transcription factors and of potential target genes in normal mammary tissue and tumors. J Biol Chem 2004, 279:11281–11292
19. Neznanov NS, Oshima RG: Cis regulation of the keratin 18 gene in transgenic mice. Mol Cell Biol 1993, 13:1815–1823
20. Oshima RG, Lesperance J, Munoz V, Hebbard L, Ranscht B, Sharan N, Muller WJ, Hauser CA, Cardiff RD: Angiogenic acceleration of Neu induced mammary tumor progression and metastasis. Cancer Res 2004, 64:169–179
21. Maglione JE, Moghanaki D, Young LJ, Manner CK, Ellies LG, Joseph SO, Nicholson B, Cardiff RD, MacLeod CL: Transgenic polyoma middle-T mice model premalignant mammary disease. Cancer Res 2001, 61:8298–8305
22. Maglione JE, McGoldrick ET, Young LJ, Namba R, Gregg JP, Liu L, Moghanaki D, Ellies LG, Borowsky AD, Cardiff RD, MacLeod CL: Polyomavirus middle T-induced mammary intraepithelial neoplasia outgrowths: single origin, divergent evolution, and multiple outcomes. Mol Cancer Ther 2004, 3:941–953
23. Webster MA, Hutchinson JN, Rauh MJ, Muthuswamy SK, Anton M, Tortorice CG, Cardiff RD, Graham FL, Hassell JA, Muller WJ: Requirement for both Shc and phosphatidylinositol 3′ kinase signaling pathways in polyomavirus middle T-mediated mammary tumorigenesis. Mol Cell Biol 1998, 18:2344–2359
24. Grippo PJ, Nowlin PS, Demeure MJ, Longnecker DS, Sandgren EP: Preinvasive pancreatic neoplasia of ductal phenotype induced by acinar cell targeting of mutant kras in transgenic mice. Cancer Res 2003, 63:2016–2019
25. Guy CT, Cardiff RD, Muller WJ: Induction of mammary tumors by expression of polyomavirus middle T oncogene: a transgenic mouse model for metastatic disease. Mol Cell Biol 1992, 12:954–961
26. Miyamoto Y, Maitra A, Ghosh B, Zechner U, Argani P, Iacobuzio-Donahue CA, Sriuranpong V, Iso T, Meszoely IM, Wolfe MS, Hruban RH, Ball DW, Schmid RM, Leach SD: Notch mediates TGF alpha-induced changes in epithelial differentiation during pancreatic tumorigenesis. Cancer Cell 2003, 3:565–576
27. Gottlieb KA, Villarreal LP: Natural biology of polyomavirus middle T antigen. Microbiol Mol Biol Rev 2001, 65:288–318
28. Siegel PM, Ryan ED, Cardiff RD, Muller WJ: Elevated expression of activated forms of Neu/ErbB-2 and ErbB-3 are involved in the induction of mammary tumors in transgenic mice: implications for human breast cancer. EMBO J 1999, 18:2149–2164
29. Dankort DL, Muller WJ: Signal transduction in mammary tumorigenesis: a transgenic perspective. Oncogene 2000, 19:1038–1044
30. Rosner A, Miyoshi K, Landesman-Bollag E, Xu X, Seldin DC, Moser AR, MacLeod CL, Shyamala G, Gillgrass AE, Cardiff RD: Pathway pathology: histological differences between ErbB/Ras and Wnt pathway transgenic mammary tumors. Am J Pathol 2002, 161:1087–1097
31. Cardiff RD: Validity of mouse mammary tumor models for human breast cancer: comparative pathology. Microsc Res Tech 2001, 52:224–230
32. Pankov R, Umezawa A, Maki R, Der CJ, Hauser CA, Oshima RG: Keratin 18 activation by Ha-ras is mediated through ets and jun binding sites. Proc Natl Acad Sci USA 1994, 91:873–877
33. Aguirre AJ, Bardeesy N, Sinha M, Lopez L, Tuveson DA, Horner J, Redston MS, DePinho RA: Activated Kras and Ink4a/Arf deficiency cooperate to produce metastatic pancreatic ductal adenocarcinoma. Genes Dev 2003, 17:3112–3126
34. Wagner M, Greten FR, Weber CK, Koschnick S, Mattfeldt T, Deppert W, Kern H, Adler G, Schmid RM: A murine tumor progression model for pancreatic cancer recapitulating the genetic alterations of the human disease. Genes Dev 2001, 15:286–293
35. Lewis BC, Klimstra DS, Varmus HE: The c-myc and PyMT oncogenes induce different tumor types in a somatic mouse model for pancreatic cancer. Genes Dev 2003, 17:3127–3138
36. Sumazaki R, Shiojiri N, Isoyama S, Masu M, Keino-Masu K, Osawa M, Nakauchi H, Kageyama R, Matsui A: Conversion of biliary system to pancreatic tissue in Hes1-deficient mice. Nat Genet 2004, 36:83–87
37. Jensen J, Pedersen EE, Galante P, Hald J, Heller RS, Ishibashi M, Kageyama R, Guillemot F, Serup P, Madsen OD: Control of endodermal endocrine development by Hes-1. Nat Genet 2000, 24:36–44
38. Tehranian A, Morris DW, Min BH, Bird DJ, Cardiff RD, Barry PA: Neoplastic transformation of prostatic and urogenital epithelium by the polyoma virus middle T gene. Am J Pathol 1996, 149:1177–1191